Understanding the Quality Factor of Mass-Loaded Tensioned Resonators

R. Shaniv, S. Kumar Keshava, C. Reetz, and C. A. Regal
(Dated: September 18, 2022)

Mechanical resonators featuring large tensile stress have enabled a range of experiments in quantum optomechanics and novel sensing. Many sensing applications require functionalizing tensioned resonators by appending additional mass to them. However, this may dramatically change the resonator mode quality factor, and hence its sensitivity. In this work, we investigate the effect of the crossover from no mass load to a large mass load on the mode shape and quality factor of a tensioned resonator. We show through an analytical model and finite element analysis that as the load mass increases, surprisingly, the resonator mode shape becomes independent of the exact load mass, and therefore, the resonator mode quality factor saturates. We validate this saturation effect experimentally by measuring the quality factor of a tensioned silicon nitride trampoline resonator while varying the load mass in a controlled manner.

Micromechanical and nanomechanical resonators have been a fruitful topic of research for several decades. They have shown promise for exploring quantum physics [1], in studies ranging from quantum transduction protocols [2–4], creation of quantum memories [5–7], to the generation of squeezed light [8–10], and for precision sensing applications, such as magnetic force detection [11–13], nanoscale imaging [14, 15], accelerometer design [16, 17], and mass sensing [18–20].

An adequate sensor requires both appreciable coupling to the physical parameter it is designed to sense and low environmental noise. An important figure of merit that quantifies the sensitivity of a resonator normal mode is the quality factor, denoted hereafter as Q. The Q depends on environmental isolation and is a measure of the number of coherent oscillations a resonator mode can provide before losing a significant portion of its energy to the environment [1, 21]. Therefore, resonator modes with utmost Q values are ideal for sensing.

To couple a resonator sensor to a quantity of interest, it is often necessary to functionalize it with a coupling agent, resulting in an additional resonator mass, e.g. magnetic particles for magnetic force sensing [11, 13] or test masses for acceleration detection [16, 17]. Certain applications, such as those that aim to measure gravitational forces, require appending a mass that is much larger than the resonator mass [22–24]. In general, specific interest is devoted to modes where the mass moves appreciably. For a large mass, typically, a single mode has a significant motion in the load, and it is usually the lowest frequency or fundamental mode. Although essential for sensing, the addition of a load mass might lower the resonator mode Q, and degrade its performance as a sensor. It is therefore of interest to understand how the Q of a resonator mode is affected by mass loading.

The Q of a resonator mode is defined as $Q = 2\pi\frac{W}{\Delta W}$, where W is the energy stored in the mode, and ΔW is the energy loss per oscillatory cycle [21]. In general, ΔW is a sum of the contributions from multiple individual loss mechanisms [25]. One way to improve the Q of a resonator is by increasing the stored energy without a similar increase in the dissipation. This can be achieved by using a tensioned or high-stress film that results in the phenomenon known as dissipation dilution [26–28]. High-stress also extends the resonator mode spectrum to higher frequencies for a given resonator length scale. High frequency is of interest for certain sensing protocols, while being out of reach for similar length scale non-tensioned resonators such as cantilevers.

Low optical absorption combined with high-stress obtained in fabrication make silicon nitride (SiN) a natural material for the design of high Q resonators [29–31]. In tensioned SiN resonator modes, typically, Q is limited by two loss mechanisms — bending loss, which is the energy lost due to the bending of the mode, and radiation loss, which is the energy lost from the mode into the surroundings via acoustic radiation. This allows us to define individual quality factors, Q_{bend} and Q_{rad}, associated with bending loss and radiation loss respectively. Therefore, we can write $\frac{1}{Q} = \frac{1}{Q_{\mathrm{bend}}} + \frac{1}{Q_{\mathrm{rad}}}$. Q_{bend} can be significantly improved by tailoring the mode shape to reduce bending loss at the mode edge, commonly referred to as clamping loss [27, 28, 32–37]. Q_{rad} can be improved by resonator patterning, substrate engineering, and strategic device mounting [27, 32, 37–44]. These techniques have led to resonators with modes limited by Q_{bend}.

In this work, we study the effect of a localized mass load on the Q_{bend} of highly tensioned resonators. We show through analytical calculations and finite element analysis (FEA) simulations that as the load mass increases, the modes of the resonator change in frequency and shape. Further, we show that for a large enough mass, each mode shape becomes independent of the mass, which leads to mass-independent Q_{bend}. We refer to this phenomenon as Q_{bend} *mass saturation*. We validate this saturation experimentally by measuring the Q of a tensioned SiN trampoline resonator [34, 36] as a function of the load mass. We use magnetic grains for the load mass, and we vary the mass by sequentially stacking the grains using their mutual magnetic attraction to avoid varying the amount of lossy adhesive used. This allows us to compare Q measurements for different load masses

on a single device.

To obtain an expression for the Q_{bend} of a mode, we assume pure out-of-plane mode displacement $u(x,y)$, where x and y are in-plane resonator coordinates, as well as small displacement, $|u(x,y)| \ll h$, where h is the resonator thickness. In addition, we assume large in-plane tensile stress σ_0, such that the speed of sound along the resonator is approximately proportional to $\sqrt{\sigma_0}$. Then we can write $W \approx \int_V \frac{\sigma_0}{2}\left[\left(\frac{\partial u}{\partial x}\right)^2 + \left(\frac{\partial u}{\partial y}\right)^2\right] dV$ and $\Delta W_{\text{bend}} \approx \int_V \frac{\pi E_2}{(1-\nu^2)} z^2 \left[\frac{\partial^2 u}{\partial x^2} + \frac{\partial^2 u}{\partial y^2}\right]^2 dV$, where E_2 is the imaginary part of the Young modulus, ν is the Poisson ratio, z is the resonator coordinate along its thickness and V is the volume of the resonator [27, 45]. This leads to:

$$Q_{\text{bend}}(u) = \frac{\int_V \sigma_0 \left[\left(\frac{\partial u}{\partial x}\right)^2 + \left(\frac{\partial u}{\partial y}\right)^2\right] dV}{\int_V \frac{E_2}{(1-\nu^2)} z^2 \left[\frac{\partial^2 u}{\partial x^2} + \frac{\partial^2 u}{\partial y^2}\right]^2 dV} \qquad (1)$$

Eq. 1 affirms that if the mode shape $u(x,y)$ is independent of the load mass, Q_{bend} saturates.

We can elucidate this Q_{bend} saturation and its origin through an example model. We study the fundamental mode of a highly tensioned suspended beam, referred to as a string, with a mass load. The string resonator is fixed at both ends, with displacement $u(x)$ in the vertical axis, where x is the coordinate along the resonator (Fig. 1a). Here $u(x)$ satisfies the string equation [25]:

$$\frac{Eh^2}{12\sigma_0}\frac{d^4u}{dx^4} - \frac{d^2u}{dx^2} - \frac{\rho(x)(2\pi f)^2}{\sigma_0}u = 0, \qquad (2)$$

for $0 \le x \le L$, where L is the string length. Here, E, h, σ_0, are the string's Young's modulus, thickness and the tensile stress respectively, and f is the mode frequency. The string width w is absent from the equation because the string has a uniform width. The position-dependent density $\rho(x)$ accounts for possible increased density at some region $a \le x \le b$, for $0 < a < b < L$. We denote the density at $0 \le x < a$ and $b < x \le L$, subsequently referred to as the outer regions, by ρ_m, and the density at $a \le x \le b$, the inner region, by $\rho_m + \rho_M$, such that ρ_M is the added density. The pre-stress σ_0 is assumed to be large, satisfying the length scale inequality $l = 2\pi\sqrt{\frac{Eh^2}{12\sigma_0}} \ll L$.

Given this high-stress, the frequency of the string's fundamental mode can be well approximated by neglecting the fourth derivative term in Eq. 2 [25]. The solution then reads:

$$u(x) = \begin{cases} A_1 \sin\left(\frac{\alpha}{\sqrt{1+\chi}}x\right) & 0 \le x \le a \\ A_2 \sin(\alpha x) + B_2 \cos(\alpha x) & a \le x \le b \\ A_3 \sin\left(\frac{\alpha}{\sqrt{1+\chi}}(L-x)\right) & b \le x \le L \end{cases}, \qquad (3)$$

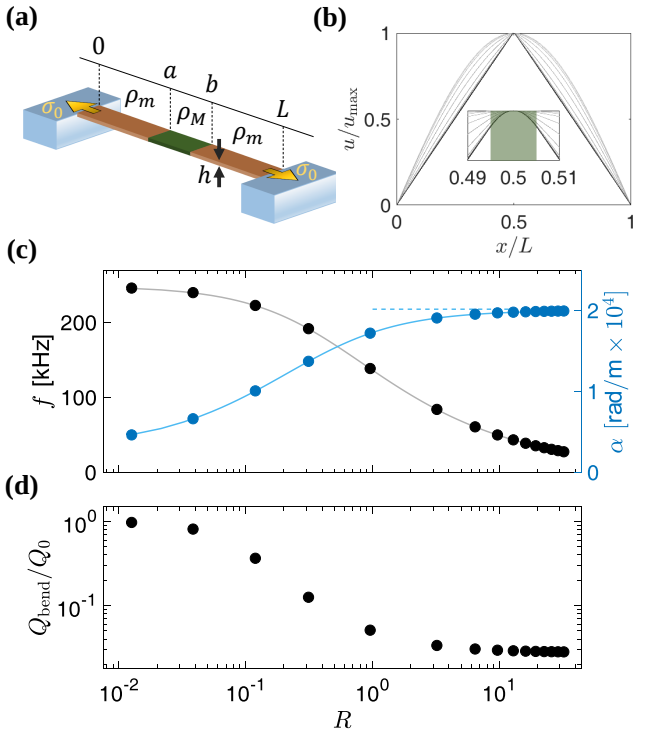

FIG. 1. **Mass loaded string theoretical model.** **(a)** String parameters: A string of length L, thickness h, with tensile stress σ_0 is fixed at points $x = 0$ and $x = L$, where x is the coordinate along the string length, and has linear density ρ_m everywhere except for the region $a \le x \le b$, where the density is $\rho_M + \rho_m$. **(b)** Mode shape visualization: FEA simulations of the mass-loaded string fundamental mode normalized to its maximum displacement (lighter color corresponds to lighter mass load) plotted against the spatial coordinate normalized to the string length. Inset: zoomed image of the mode shape around the mass loaded region (shaded green). **(c)** String frequency and inner region wavenumber: FEA simulated (solid circles) and analytically calculated (solid lines) fundamental mode frequency (black) and inner region wavenumber (blue) of a string are shown as a function of R, the ratio between the mass of the load and the total mass of the unloaded resonator. FEA simulation points correspond to the different mode shapes in subfigure **(b)**. Dashed blue line is the analytically calculated large mass limit inner region wavenumber α_{lim}. **(d)** String quality factor: The fundamental mode Q_{bend} normalized to Q_0, the Q_{bend} of an unloaded resonator, as a function of the mass ratio R. To focus on the effect of the mass load, Q_{bend} was calculated without the mechanical clamping loss contribution from the mode edges. Subfigures **(c)** and **(d)** share the same horizontal coordinate, and results shown correspond to specific choice of parameters (supplementary material).

where we introduced the density ratio $\chi = \frac{\rho_M}{\rho_m}$ and the inner region wavenumber $\alpha = 2\pi f\sqrt{\frac{\rho_m+\rho_M}{\sigma_0}}$, and imposed the fixed boundary conditions $u(0) = u(L) = 0$. An equation for α can be found by using the continuity of $u(x)$ and its first derivative at $x = a$ and $x = b$ (supplementary material). We see excellent agreement (Fig. 1c)

between FEA simulations of α and f, and the corresponding numerically-evaluated analytical calculation, for different values of R, the resonator mass ratio, which we define as $R = \frac{M_{\text{load}}}{M_{\text{unloaded}}}$. Here, $M_{\text{load}} = hw\,(b-a)\,(\rho_M)$ and $M_{\text{unloaded}} = hwL\rho_m$ correspond to the load mass and the total unloaded resonator mass, respectively. This parameter was chosen to emphasize that we are investigating the crossover between no load ($R = 0$) and a load significantly larger than the entire resonator mass ($R \gg 1$).

In addition to α and f, we used the results from the FEA simulations for the fundamental mode along with Eq. 1 to calculate Q_{bend}/Q_0 as a function of R (Fig. 1d). Here, Q_0 is simply the Q_{bend} of the unloaded resonator. In order to focus on the effect of the load mass, we excluded the mechanical clamping loss contribution from the mode edges. We find that Q_{bend}/Q_0 becomes independent of the exact load mass for $R \gg 1$ and it saturates to a value lower than when R is close to zero.

Fig. 1b evinces that the fundamental mode inner region wavenumber α saturates to a finite value, α_{lim}, as the mass grows larger (supplementary material). Simultaneously, the outer region wavenumber diminishes, and in the large mass limit the mass loaded string equation can be approximated as

$$\frac{l^2}{(2\pi)^2}\frac{d^4u}{dx^4} - \frac{d^2u}{dx^2} - K^2\,(x)\,u = 0, \tag{4}$$

where

$$K^2(x) \approx \begin{cases} 0 & 0 \le x < a, \quad b < x \le L \\ \alpha_{\text{lim}}^2 & a \le x \le b \end{cases} \tag{5}$$

Because this equation is independent of the load mass, so is its solution (supplementary material).

In the high mass load limit, the shape of the unloaded regions can be understood in two equivalent ways. The first is temporal: for an unloaded resonator, the fundamental mode period is given by $T_{\text{unloaded}} = \sqrt{\frac{\rho_m}{\sigma_0}}2L$, which is the time it takes an out-of-plane mechanical perturbation to make a roundtrip across a resonator of length L, with speed of sound $\sqrt{\frac{\sigma_0}{\rho_m}}$. As the high mass load limit is approached ($\rho_m \to \rho_m + \rho_M$), the mode period increases to T_{loaded}, which is now much longer than the roundtrip time taken for a perturbation to propagate in the unloaded regions. As a result, the mode shape in the unloaded region approximates a quasi-static displacement, with the limit shape being a static displacement at any moment. The second explanation is spatial: in the limit of a large load mass, the mode wavelength in the unloaded region, $T_{\text{loaded}}\sqrt{\frac{\sigma_0}{\rho_m}}$, is much longer than the unloaded region length scale. As a result, the mode shape converges to a displacement function that does not curve in the unloaded region. For a string, the resulting limit shape is linear in the outer regions, and since the inner region has to match with the outer regions at the boundaries, the overall mode approaches a limit shape that is approximately triangular (Fig. 1b). This leads to the splitting of the string equation as is described in Eq. 4 and Eq. 5, and as explained, its solution is independent of the load mass, leading to Q_{bend} saturation.

Although our analysis thus far has focused on the case of the mass loaded string, the key points of the explanation above apply more generally to highly tensioned resonators of arbitrary geometry and imply Q_{bend} saturation for a high enough mass load. Specifically, as an example we have also analyzed a circular membrane (supplementary material).

To validate the model-predicted Q_{bend} saturation effect experimentally, we measured the fundamental mode Q, denoted hereafter as Q_{fund}, of a high-stress SiN trampoline resonator for different load masses [34, 36]. A trampoline resonator features a wide pad for low-imprecision optical detection and the geometry is designed to reduce mechanical clamping losses [34, 36]. Our device was mounted on a custom-made silicon base to minimize radiation loss. This setup ensured $Q_{\text{rad}} \gg Q_{\text{bend}}$ for an unloaded trampoline fundamental mode, and thus allowed $Q_{\text{fund}} \approx Q_{\text{bend}}$ (supplementary material).

In order to vary the load mass while keeping the other variables constant, we employed a "magnetic stacking" technique using magnetic particles as the load mass. The first particle was affixed to our device using ultra-violet (UV) cured epoxy (NEA 123SHGA) (Fig. 2a) and then magnetized strongly using an external field. Next, a second particle was brought near the first, resulting in magnetic attraction between the particles. A strong field was applied once again to magnetize the second particle, making both particles a single, inseparable mass without using additional epoxy. This procedure was repeated (Fig. 2c) and Q_{fund} was measured between each addition of mass. Although we expected the epoxy to have high mechanical loss compared to SiN, by keeping its geometry constant through magnetic stacking, we could study how Q_{fund} is affected by mass loading while avoiding errors associated with multiple epoxy applications.

The key experimental results are shown in Fig. 3a along with relevant FEA simulations. The open black circle and solid black circles correspond to the measured Q_{fund} values for a trampoline resonator at 300 K, without and with a variable load mass, respectively. As visible, Q_{fund} decreases as the load mass increases, but becomes insensitive at higher load mass values. This is manifested as a plateau for masses larger than $\sim$ 10 ng. This saturated Q_{fund} value is approximately four orders of magnitude lower than the unloaded Q_{fund}. To model these results, we used FEA simulations that accounted for bending loss in both the SiN and the epoxy, while disregarding radiation loss (black dotted line). We scanned the epoxy length scale and loss tangent and chose realistic

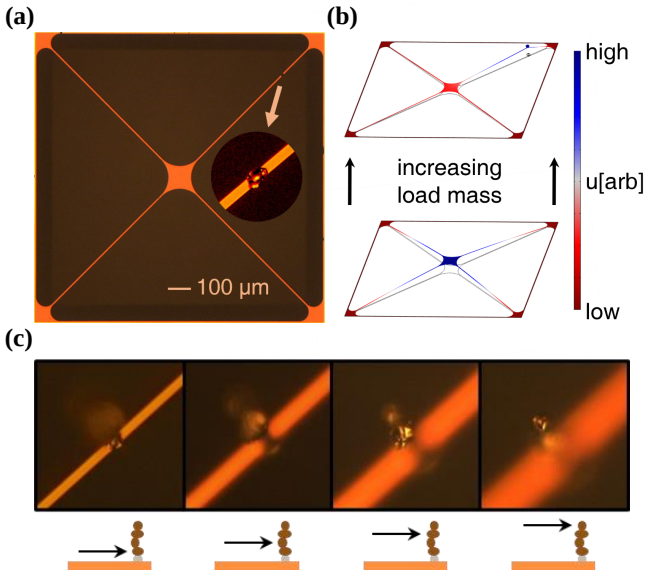

FIG. 2. **System for experimental validation.** **(a)** Microscope image of device: Optical image of the trampoline resonator with a magnet on its tether, and a zoomed image of the magnet (inset). **(b)** Mode shape visualization: FEA simulations show the trampoline fundamental mode shape with both a high mass load (top) and without a mass load (bottom). **(c)** Magnetic stacking: Images in different planes of focus show a stack of four magnets, from the first magnet in focus (leftmost image) to the fourth magnet in focus (rightmost image). The drawing at the bottom shows a side-view of the trampoline resonator (orange slab) with a droplet of epoxy (grey dot) and a stack of magnets (dark brown dot). Each drawing indicates the magnet in focus in the corresponding image (black arrow pointing at dark brown dot).

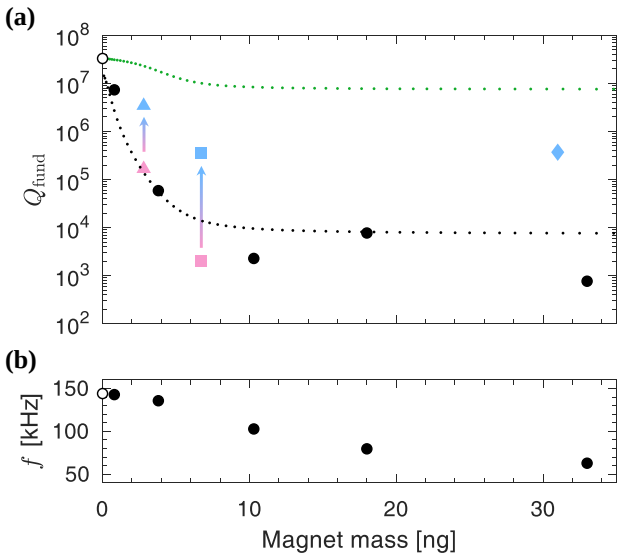

FIG. 3. **Experimental results and FEA simulations.** **(a)** Trampoline Q_{fund} as a function of magnet mass: Experimentally measured Q_{fund} at 300 K (circles) without a load mass (open black circle), and with a varying load mass (solid black circles). Corresponding FEA simulated Q_{bend} results at 300 K are shown when bending loss in the epoxy is disregarded (green dotted line), and when bending loss in the epoxy is accounted for (black dotted line). Experimentally measured Q_{fund} values for two other devices (triangle and square) are shown at both 300 K (light pink) and 8 K (sky blue). The first device (triangle) has mass load of 2.8 ng and the second device (square) has mass load of 6.7 ng. Experimentally measured Q_{fund} for a third device (diamond) at 8 K (sky blue) with a large load mass of 31.0 ng is also shown. **(b)** Trampoline fundamental mode frequency as a function of magnet mass: Experimental frequency measurements at 300 K (circles) without a load mass (open black circle) and with a varying load mass (solid black circles). Subfigures **(a)** and **(b)** share the same horizontal coordinate.

model parameters to obtain reasonable agreement between our simulation results and measured data, while also setting an upper bound on Q_{fund} (supplementary material). However, our simulated model does not fit all the data points to within the measurement noise, which we believe is because, irrespective of device mounting, at higher mass (lower frequency), the resonator is more susceptible to radiation loss.

In order to further validate that the large reduction in Q_{fund} originates mainly from loss in the epoxy rather than radiation loss, we performed additional measurements on two different devices (triangle and square) both at temperatures of 300 K and 8 K (light pink and sky blue markers respectively). The results show that the Q_{fund} rises by about two orders of magnitude for resonators cooled to 8 K. Although SiN resonators are expected to have reduced bending loss at 8 K compared to 300 K, empirically it is by a small factor of ~ 3, which cannot explain the measured difference in Q_{fund} [32]. We therefore conclude that when cold, the epoxy's bending loss reduces significantly, affirming the reduction in Q_{fund} (open black circle and solid black circles) is primarily due to loss in the epoxy.

A fourth device (sky blue diamond) measured at 8 K provides evidence that a fairly high quality factor ($Q_{\mathrm{fund}} \approx 3.7 \times 10^5$) can be achieved in the saturated regime. Previous studies have shown that using better epoxy can lead to higher quality factors [46].

In order to set a theoretical limit on the saturated Q_{fund} at 300 K, we performed FEA simulations that include only SiN bending loss and disregard all other forms of loss (green dotted line). The results indicate it is possible to obtain a Q_{bend} decrease of only a factor of ~ 1.5 (Q_{bend} as high as 10^7) in the limit of a large load mass. The saturated Q_{bend} for trampolines can be further optimized by changing the location of local mass loading (supplementary material), and possibly by using trampoline resonators with carefully engineered geometries [34, 36, 47].

In conclusion, we have analyzed the problem of ten-

sioned mechanical resonators with a local mass load. We have demonstrated theoretically and experimentally that for a large load mass, the mode shape becomes independent of the mass and converges to a limit shape, implying that Q_{bend} saturates. We believe that this work provides important guiding principles for the design of sensors where mass loading is needed, such as in magnetic field sensors [11–13], accelerometers [16, 17], mass balances [18–20], and gravity detectors [22–24, 48]. Further, the ideas presented could be extended to other high Q tensioned two dimensional devices such as phononic crystals [27, 32, 38], hierarchical structures [35, 49], and machine-learning optimized resonators [47, 50].

We thank M. Urmey for helpful comments on the manuscript. This work was supported by funding from NSF Grant No. PHYS 1734006, Cottrell FRED Award from the Research Corporation for Science Advancement under grant 27321, and the Baur-SPIE Endowed Professor at JILA.

[1] Aspelmeyer, M., Kippenberg, T. & Marquardt, F. Cavity optomechanics. *Reviews Of Modern Physics*. **86**, 1391 (2014)

[2] Andrews, R., Peterson, R., Purdy, T., Cicak, K., Simmonds, R., Regal, C. & Lehnert, K. Bidirectional and efficient conversion between microwave and optical light. *Nature Physics*. **10**, 321-326 (2014)

[3] Forsch, M., Stockill, R., Wallucks, A., Marinković, I., Gärtner, C., Norte, R., Otten, F., Fiore, A., Srinivasan, K. & Gröblacher, S. Microwave-to-optics conversion using a mechanical oscillator in its quantum ground state. *Nature Physics*. **16**, 69-74 (2020)

[4] Mirhosseini, M., Sipahigil, A., Kalaee, M. & Painter, O. Superconducting qubit to optical photon transduction. *Nature*. **588**, 599-603 (2020)

[5] Wallucks, A., Marinković, I., Hensen, B., Stockill, R. & Gröblacher, S. A quantum memory at telecom wavelengths. *Nature Physics*. **16**, 772-777 (2020)

[6] Kharel, P., Chu, Y., Power, M., Renninger, W., Schoelkopf, R. & Rakich, P. Ultra-high-Q phononic resonators on-chip at cryogenic temperatures. *Apl Photonics*. **3**, 066101 (2018)

[7] MacCabe, G., Ren, H., Luo, J., Cohen, J., Zhou, H., Sipahigil, A., Mirhosseini, M. & Painter, O. Nano-acoustic resonator with ultralong phonon lifetime. *Science*. **370**, 840-843 (2020)

[8] Purdy, T., Yu, P., Peterson, R., Kampel, N. & Regal, C. Strong optomechanical squeezing of light. *Physical Review X*. **3**, 031012 (2013)

[9] Safavi-Naeini, A., Gröblacher, S., Hill, J., Chan, J., Aspelmeyer, M. & Painter, O. Squeezed light from a silicon micromechanical resonator. *Nature*. **500**, 185-189 (2013)

[10] Brooks, D., Botter, T., Schreppler, S., Purdy, T., Brahms, N. & Stamper-Kurn, D. Non-classical light generated by quantum-noise-driven cavity optomechanics. *Nature*. **488**, 476-480 (2012)

[11] Rugar, D., Budakian, R., Mamin, H. & Chui, B. Single spin detection by magnetic resonance force microscopy. *Nature*. **430**, 329-332 (2004)

[12] Scozzaro, N., Ruchotzke, W., Belding, A., Cardellino, J., Blomberg, E., McCullian, B., Bhallamudi, V., Pelekhov, D. & Hammel, P. Magnetic resonance force detection using a membrane resonator. *Journal Of Magnetic Resonance*. **271** pp. 15-20 (2016)

[13] Fischer, R., McNally, D., Reetz, C., Assumpcao, G., Knief, T., Lin, Y. & Regal, C. Spin detection with a micromechanical trampoline: towards magnetic resonance microscopy harnessing cavity optomechanics. *New Journal Of Physics*. **21**, 043049 (2019)

[14] Degen, C., Poggio, M., Mamin, H., Rettner, C. & Rugar, D. Nanoscale magnetic resonance imaging. *Proceedings Of The National Academy Of Sciences*. **106**, 1313-1317 (2009)

[15] Hälg, D., Gisler, T., Tsaturyan, Y., Catalini, L., Grob, U., Krass, M., Héritier, M., Mattiat, H., Thamm, A., Schirhagl, R. & Others Membrane-based scanning force microscopy. *Physical Review Applied*. **15**, L021001 (2021)

[16] Krause, A., Winger, M., Blasius, T., Lin, Q. & Painter, O. A high-resolution microchip optomechanical accelerometer. *Nature Photonics*. **6**, 768-772 (2012)

[17] Zhou, F., Bao, Y., Madugani, R., Long, D., Gorman, J. & LeBrun, T. Broadband thermomechanically limited sensing with an optomechanical accelerometer. *Optica*. **8**, 350-356 (2021)

[18] Yang, Y., Callegari, C., Feng, X., Ekinci, K. & Roukes, M. Zeptogram-scale nanomechanical mass sensing. *Nano Letters*. **6**, 583-586 (2006)

[19] Ekinci, K., Huang, X. & Roukes, M. Ultrasensitive nanoelectromechanical mass detection. *Applied Physics Letters*. **84**, 4469-4471 (2004)

[20] Lavrik, N. & Datskos, P. Femtogram mass detection using photothermally actuated nanomechanical resonators. *Applied Physics Letters*. **82**, 2697-2699 (2003)

[21] Taylor, J. Classical Mechanics. 3 "E ed. (Print)

[22] Liu, Y., Mummery, J., Zhou, J. & Sillanpää, M. Gravitational forces between nonclassical mechanical oscillators. *Physical Review Applied*. **15**, 034004 (2021)

[23] Schmöle, J., Dragosits, M., Hepach, H. & Aspelmeyer, M. A micromechanical proof-of-principle experiment for measuring the gravitational force of milligram masses. *Classical And Quantum Gravity*. **33**, 125031 (2016)

[24] Pratt, J., Agrawal, A., Condos, C., Pluchar, C., Schlamminger, S. & Wilson, D. Nanoscale torsional dissipation dilution for quantum experiments and precision measurement. *ArXiv Preprint ArXiv:2112.08350*. (2021)

[25] Schmid, S., Villanueva, L. & Roukes, M. Fundamentals of nanomechanical resonators. (Springer,2016)

[26] Fedorov, S., Engelsen, N., Ghadimi, A., Bereyhi, M., Schilling, R., Wilson, D. & Kippenberg, T. Generalized dissipation dilution in strained mechanical resonators. *Physical Review B*. **99**, 054107 (2019)

[27] Tsaturyan, Y., Barg, A., Polzik, E. & Schliesser, A. Ultracoherent nanomechanical resonators via soft clamping and dissipation dilution. *Nature Nanotechnology*. **12**, 776-783 (2017)

[28] Ghadimi, A., Fedorov, S., Engelsen, N., Bereyhi, M., Schilling, R., Wilson, D. & Kippenberg, T. Elastic strain engineering for ultralow mechanical dissipation. *Science*. **360**, 764-768 (2018)

[29] Zwickl, B., Shanks, W., Jayich, A., Yang, C., Bleszynski Jayich, A., Thompson, J. & Harris, J. High quality mechanical and optical properties of commercial silicon

nitride membranes. *Applied Physics Letters.* **92**, 103125 (2008)

[30] Yuan, M., Cohen, M. & Steele, G. Silicon nitride membrane resonators at millikelvin temperatures with quality factors exceeding 108. *Applied Physics Letters.* **107**, 263501 (2015)

[31] Serra, E., Bawaj, M., Borrielli, A., Di Giuseppe, G., Forte, S., Kralj, N., Malossi, N., Marconi, L., Marin, F., Marino, F. & Others Microfabrication of large-area circular high-stress silicon nitride membranes for optomechanical applications. *AIP Advances.* **6**, 065004 (2016)

[32] Reetz, C., Fischer, R., Assumpcao, G., McNally, D., Burns, P., Sankey, J. & Regal, C. Analysis of membrane phononic crystals with wide band gaps and low-mass defects. *Physical Review Applied.* **12**, 044027 (2019)

[33] Bereyhi, M., Beccari, A., Fedorov, S., Ghadimi, A., Schilling, R., Wilson, D., Engelsen, N. & Kippenberg, T. Clamp-tapering increases the quality factor of stressed nanobeams. *Nano Letters.* **19**, 2329-2333 (2019)

[34] Reinhardt, C., Müller, T., Bourassa, A. & Sankey, J. Ultralow-noise SiN trampoline resonators for sensing and optomechanics. *Physical Review X.* **6**, 021001 (2016)

[35] Fedorov, S., Beccari, A., Engelsen, N. & Kippenberg, T. Fractal-like mechanical resonators with a soft-clamped fundamental mode. *Physical Review Letters.* **124**, 025502 (2020)

[36] Norte, R., Moura, J. & Gröblacher, S. Mechanical resonators for quantum optomechanics experiments at room temperature. *Physical Review Letters.* **116**, 147202 (2016)

[37] Ghadimi, A., Wilson, D. & Kippenberg, T. Radiation and internal loss engineering of high-stress silicon nitride nanobeams. *Nano Letters.* **17**, 3501-3505 (2017)

[38] Yu, P., Cicak, K., Kampel, N., Tsaturyan, Y., Purdy, T., Simmonds, R. & Regal, C. A phononic bandgap shield for high-Q membrane microresonators. *Applied Physics Letters.* **104**, 023510 (2014)

[39] Weaver, M., Pepper, B., Luna, F., Buters, F., Eerkens, H., Welker, G., Perock, B., Heeck, K., Man, S. & Bouwmeester, D. Nested trampoline resonators for optomechanics. *Applied Physics Letters.* **108**, 033501 (2016)

[40] Norte, R. Nanofabrication for On-Chip Optical Levitation, Atom-Trapping, and Superconducting Quantum Circuits. *PhD Thesis.* (2015)

[41] Wilson, D. Cavity Optomechanics with High-Stress Silicon Nitride Films. *PhD Thesis.* (2012)

[42] Reinhardt, C. Ultralow-Noise Silicon Nitride Trampoline Resonators for Sensing and Optomechanics. *PhD Thesis.* (2017)

[43] Borrielli, A., Marconi, L., Marin, F., Marino, F., Morana, B., Pandraud, G., Pontin, A., Prodi, G., Sarro, P., Serra, E. & Others Control of recoil losses in nanomechanical SiN membrane resonators. *Physical Review B.* **94**, 121403 (2016)

[44] Li, Z., Zhang, Q., You, X., Li, Y. & Peng, K. Suppression of phonon tunneling losses by microfiber strings for high-Q membrane microresonators. *Applied Physics Letters.* **109**, 191903 (2016)

[45] Yu, P., Purdy, T. & Regal, C. Control of material damping in high-Q membrane microresonators. *Physical Review Letters.* **108**, 083603 (2012)

[46] Schediwy, S., Gras, S., Ju, L. & Blair, D. High Q factor bonding using natural resin for reduced thermal noise of test masses. *Review Of Scientific Instruments.* **76**, 026117 (2005)

[47] Høj, D., Wang, F., Gao, W., Hoff, U., Sigmund, O. & Andersen, U. Ultra-coherent nanomechanical resonators based on inverse design. *Nature Communications.* **12**, 1-8 (2021)

[48] González, G. & Saulson, P. Brownian motion of a mass suspended by an anelastic wire. *The Journal Of The Acoustical Society Of America.* **96**, 207-212 (1994)

[49] Bereyhi, M., Beccari, A., Groth, R., Fedorov, S., Arabmoheghi, A., Kippenberg, T. & Engelsen, N. Hierarchical tensile structures with ultralow mechanical dissipation. *Nature Communications.* **13**, 1-9 (2022)

[50] Shin, D., Cupertino, A., Jong, M., Steeneken, P., Bessa, M. & Norte, R. Spiderweb nanomechanical resonators via bayesian optimization: inspired by nature and guided by machine learning. *Advanced Materials.* **34**, 2106248 (2022)